Agricultural and Forest Meteorology, 52 (1990) 45–69
Elsevier Science Publishers B.V., Amsterdam — Printed in The Netherlands

Remote estimation of soil moisture availability and fractional vegetation cover for agricultural fields

Toby N. Carlson[1], Eileen M. Perry[2] and Thomas J. Schmugge[3]
[1]*Department of Meteorology, The Pennsylvania State University, University Park, PA 16802 (U.S.A.)*
[2]*USDA/ARS, Tucson, AZ 85719 (U.S.A.)*
[3]*Hydrology Laboratory, USDA/ARS, Beltsville, MD 20705 (U.S.A.)*

(Received July 3, 1989; revision accepted December 12, 1989)

ABSTRACT

Carlson, T.N., Perry, E.M. and Schmugge, T.J., 1990. Remote estimation of soil moisture availability and fractional vegetation cover for agricultural fields. *Agric. For. Meteorol.*, 52: 45–69.

The purpose of this paper is to present a method for using remote measurements to estimate vegetation fraction, surface energy fluxes and the root zone and soil surface water contents for partial vegetation canopies. The primary tools are a boundary layer model with vegetation and substrate components and two image products: the variation of surface radiometric temperature vs. normalized difference vegetation index (NDVI), and the standard deviation of radiometric surface temperature vs. radiometric surface temperature. The method is based on determining: (1) asymptotic values of two radiometric surface temperatures for sunlit bare soil and for dense sunlit vegetation; and (2) a relationship between NDVI and surface temperature, which we call the axis of variation. The method is illustrated using aircraft and surface measurements made at Lubbon during the French HAPEX field experiment (1986).

INTRODUCTION

Models for estimating the surface turbulent energy fluxes and the soil moisture generally depend on a sensitivity of the surface radiometric temperature to soil water content. Over bare soil, variations in radiometric surface temperature tend to be highly correlated with variations in surface water content (Jackson et al., 1977; Schmugge, 1978; Jackson, 1982). Various models have been constructed to exploit the relationship between surface temperature and soil moisture. When used in conjunction with remote measurements of surface temperature, such as determined from a satellite, these models yield estimates of the surface moisture availability, the surface energy fluxes and the thermal inertia (Carlson and Boland, 1978; Carlson et al., 1981; Price, 1982;

0168-1923/90/$03.50 © 1990 Elsevier Science Publishers B.V.

Hatfield et al., 1984; Raffy and Becker, 1985; Taconet et al., 1986; Wetzel and Woodward, 1987; Lagouarde and Choisnel, 1990). Some of these models also take into account a layer of vegetation (Taconet et al., 1986; Wetzel and Woodward, 1987; Lagouarde and Choisnel, 1990).

The relationship between soil moisture and surface temperature is vastly more complex over vegetation than over bare soil. Over vegetation there is a considerable amount of temperature variability owing to the structure of the vegetation canopy and particularly to the amount of bare soil viewed by the radiometer and exposed to the direct solar beam. Leaves tend to be cooler than the exposed bare soil because the intercellular airspaces are nearly saturated with water vapor, which is drawn from a relatively deep soil layer, the root zone. Bare soil temperatures reflect the soil moisture only over the top one or two centimeters (Idso et al., 1975).

Emitted surface radiance constitutes a blend of radiances emitted from either shaded or unshaded bare soil and vegetation. Thus, radiometric surface temperature variations over vegetated surfaces may be the result of variations in the amount of bare soil visible to the radiometer. The situation is complicated further by the problems introduced by canopy architecture, which includes the variation in solar elevation angle and viewing angle of the radiometer.

A significant step in the direction of modeling sparse or patchy vegetation cover was taken by Shuttleworth and Wallace (1985) who adapted the Penman–Monteith equation (Monteith, 1975) to account for energy partitioning between crop and soil. In order to circumvent the inconsistency of using a one-dimensional model to represent horizontally inhomogeneous surfaces, Shuttleworth and Wallace introduced the idea of two asymptotic temperature limits, one for bare soil and the other for vegetation. Their model was expressed as separate bare soil and vegetation components with identical ambient conditions above the crop. Latent heat fluxes from each of the components were combined using weighting factors, which were expressed in terms of combinations of soil and plant resistances determined from a knowledge of crop height and leaf area index (LAI).

Shuttleworth and Wallace recognized that the intractable complexity of a vegetation canopy required that they make simplifications that allow them to avoid confronting the aspects of the three-dimensional canopy. While not dismissing the effects of vegetation structure on the interception of solar radiation, they proposed that much of the fine-scale detail of the three-dimensional canopy would tend to cancel over time, leaving the first-order effects to be represented by a one-dimensional model.

Stated differently, the fluxes over bare soil are relatively independent of the adjacent vegetation (and vice versa), but are linked via common substrate and atmospheric properties. In such a geometry, LAI has two values, one for the ensemble of vegetation clumps and one for the ensemble of vegetation

clumps and contiguous bare patches. The one-dimensional model operates separately in each regime; bare soil and vegetation. Total fluxes for the combined bare soil and vegetation are related through an additional parameter, the fractional vegetation cover.

We propose a similar approach to that of Shuttleworth and Wallace, in which a boundary layer model is used in conjunction with remote measurements of surface temperature and normalized difference vegetation index (NDVI) to calculate fractional vegetation cover, LAI, substrate water content in two layers, and surface energy fluxes. The method is illustrated using remote measurements made during the French HAPEX/MOBILHY field experiment.

THE BOUNDARY LAYER MODEL

Like Shuttleworth and Wallace, we will ignore the intractable aspects of the three-dimensional canopy, and imagine a simple structure in which clumps of vegetation (which may consist of a single plant) are interspersed with bare soil patches (Fig. 1). Within the vegetation clumps, no direct solar radiation reaches the ground and no bare soil is visible to the radiometer. Uniformly distributed sparse vegetation and small dense clumps of vegetation are separated, perhaps randomly, by bare soil. The fractional part of the surface covered by the vegetation clumps is f_v and that covered by bare soil is $(1-f_v)$. No distinction is made between sunlit and shaded vegetation or between sunlit and shaded soil visible to the radiometer, although shaded bare soil may be much cooler than unshaded bare soil. Vegetation fraction also depends on the viewing angle of the radiometer; it will effectively increase with decreas-

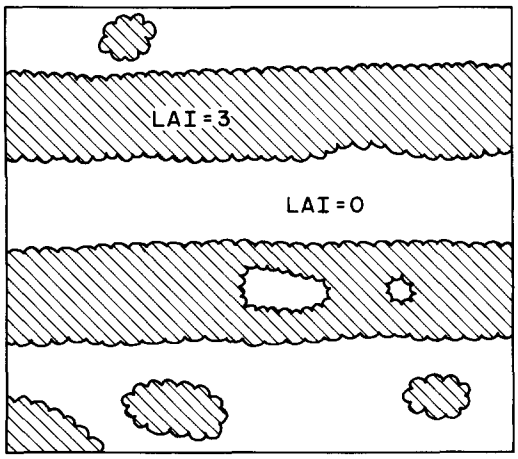

Fig. 1. Schematic view of a partial vegetation cover with leaf area index (LAI) equal to 3.0 in contiguous vegetation patches (hatching). Area represents that of a single pixel or combination of pixels.

ing elevation angle of the radiometer. This variation of f_v with viewing angle is not considered.

Since the details of the boundary layer model are not as important as the technique of applying such a model to the estimation of fractional vegetation cover and soil moisture, we will present only the basic elements of the architecture and equations; the reader is referred to Carlson et al. (1981) and Taconet et al. (1986) for a discussion of the bare soil and vegetation components, respectively. Results presented in this paper should be reproducible with any comparable model, e.g. that of Wetzel and Woodward (1987). Henceforth, the boundary layer model will be referred to as the CM. An overview of the plant and substrate structure in the CM is presented in Fig. 2.

The CM contains a single layer of vegetation, and interleaf air layer, two soil layers, a surface and a mixing layer. Fractional vegetation cover (f_v) is specified for a mixture of bare soil and vegetation. In the vegetation component, vegetation density is expressed in terms of LAI. Bare soil and vegetation regimes are calculated separately, but allowed to interact through exchanges of momentum, heat and water vapor with a common surface air layer above the canopy and a common substrate below.

Downward solar flux (S) and downward long-wave radiation ($R_l\downarrow$) are identical over both bare soil and vegetation regimes. Surface fluxes of sensible and latent heat and upward fluxes of long-wave radiation for bare soil and vegetation ($R_{lb}\uparrow$ and $R_{lv}\uparrow$) are determined separately for each regime. Radiometric temperature of the canopy (T_c) is computed from a weighted average of bare soil and vegetation components of upward long-wave radiation fluxes.

The flow of water vapor and sensible heat is expressed as follows. In the vegetation, latent heat flux (LE_f) passes from the inside of the leaf at leaf temperature (T_l) and specific humidity ($q_l(T_l)$) to the interleaf air spaces,

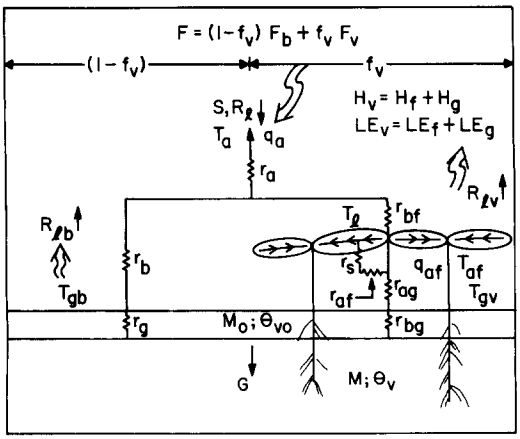

Fig. 2. Overview of plant canopy model. Fractional vegetation cover is f_v and the weighting for fluxes (F) is given by the formula at the top. The remaining symbols are defined in text.

which have a specific humidity (q_{af}), through the stomatal and the leaf boundary layer resistances (r_s; r_{af}). Stomatal resistance is calculated from a knowledge of substrate water content, incident solar flux and LAI. Sensible heat flux (H_f) passes from the leaf (at temperature (T_l)) to the interleaf air spaces, which are at temperature (T_{af}), through the leaf boundary layer resistance (r_{af}).

At the soil surface below the plants, latent heat flux (LE_g) passes from the ground surface beneath the canopy, which is at temperature (T_{gv}), to the interleaf air space through surface resistance (r_{bg}) and interleaf air space resistance (r_{ag}). Sensible heat flux (H_g) passes from the ground across resistors (r_{ag}) between the ground temperature and the interleaf air space temperature (T_{af}). These parallel fluxes (LE_f; LE_g; H_f; H_g) sum to the total vegetation fluxes of latent and sensible heat (LE_v; H_v) at the top of the vegetation canopy and pass through the canopy boundary layer resistance (r_{bf}) and the surface layer resistance (r_a).

Similarly, the calculation of fluxes over bare soil patches is simpler, but expressed in the same notation as over vegetation. Latent heat flux passes from the substrate through a soil resistance (r_g), a boundary layer resistance (r_b) and a surface layer resistance (r_a). Sensible heat flux passes from the ground surface at temperature T_{gb} directly to the atmospheric surface layer through the resistors (r_b) and (r_a). The reader is referred to Taconet et al. (1986) for further details concerning the model.

For a mixture of solid vegetation and bare soil patches, fluxes of sensible and latent heat and the upward flux of long-wave radiation above the plant canopy and the substrate heat flux (G) are taken as weighted averages of the bare soil and vegetation components, according to the vegetation fraction (f_v) using the weighting equation shown in Fig. 2. Temperature and specific humidity at the top of the surface layer (T_a; q_a) and the temperature and water content in the soil are identical for both bare soil and vegetation fractions. Air resistances for both vegetation and bare soil fractions depend on the wind speed and temperature above the canopy and therefore, indirectly, on conditions in both the vegetation and bare soil components. Radiometric temperature of the canopy (T_c) is determined from the weighted upwelling long-wave radiation flux.

An important parameter in the model is the moisture availability, which is defined for the soil surface layer with volumetric water content θ_{vo} as

$$M_o = \theta_{vo}/\theta_{sat} = (r_a + r_b)/(r_g + r_a + r_b)$$
$$= (r_a + r_{bf})/(r_{bg} + r_a + r_{bf}) \quad (1)$$

and for the root zone water content as

$$M = \theta_v/\theta_{sat} \quad (2)$$

where θ_{sat} is the volumetric water content of the soil at field capacity (θ_v). Moisture availability, the primary moisture parameter, is also defined for the surface air layer as the ratio of evaporation to potential evaporation. It should be noted that M_o, is identical for both bare soil and vegetation dominants. Since r_b and r_{bf} are calculated, eqn. (1) imposes small differences in the values of r_g and r_{bg}, which are not directly employed. Further, there is some contention in the idea that M_o can be directly equated to soil water content, although it is generally agreed that the former depends closely on the latter.

MEASUREMENTS

The HAPEX field experiment

The HAPEX-MOBILITY (Hydrologic Atmospheric Pilot Experiment and Modelisation du Bilan Hydrique) program was conducted over a 100 km by 100 km square, located within an agricultural region over southwestern France during the summer of 1986 (Andre' et al., 1988). Its main purpose was to study the hydrological budget and evaporation fluxes at the scale of a General Circulation Model. At network of rain gauges, flux-measuring devices and conventional meteorological observations, supported by aircraft and additional ground surface measurements were made during an intensive phase which lasted from May until mid-July 1986.

One of the programs in HAPEX was directed jointly by Penn State (PSU), the Centre de Recherches en Physique de l'Environment (CRPE) and the Institut National de Recherches Agronomique (INRA) to study the evolution of various plant parameters (stomatal resistance, leaf water potential, LAI, crop height) and their relationship to substrate water content and radiometric surface temperature during the intensive phase of HAPEX. PSU ground measurements were made in two fields of corn, one near the town of Lubbon (in Field N6) in the north of the test area and the other near the town of Castelnau in the south. The former was situated in a field of corn with sandy soil, within a large clearing surrounded by a forest (Les Landes); the latter was located in a corn field on a ridge. Soil water content was measured once or twice daily using gypsum blocks. These devices were calibrated at both sites by gravimetric methods, both in situ and in separate pots of soil. Additional soil water measurements were made periodically by PSU, INRA and NASA groups at this and other sites using gravimetric sampling or neutron probe. Unfortunately, because of late planting due to wet weather, the corn at Castelnau did not emerge until mid-June. Consequently, the focus of this paper is on the Lubbon measurements.

The aircraft program consisted of a series of 16 flights with a NASA C-130 aircraft over the target area during the intensive phase of HAPEX. Two multispectral scanners covering the wavelength region from the visible to the ther-

mal infrared and 21-cm microwave radiometer were mounted aboard this aircraft. Fifteen flights were made at 300 m and 1500 m; additional high altitude (6000 m) flights were made for the purpose of comparison with satellite measurements. One of the scanners was the Thermal Infrared Multi-Spectral Scanner (TIMS) and the other one the NS001 scanner which was functioning at solar wavelengths only (Schmugge and Janssen, 1988). Overflights at Lubbon were made at approximately 11:30 h local time (LST). The focus of this paper is on 4 days during the HAPEX experiment, 6, 16 and 27 June and 2 July. These were the only days in which flights were made during clear or nearly clear sky conditions.

Radiometric temperatures

Temperature measurements were obtained in an across-track scanning mode in the form of digital (DN) counts interpolated between cold and hot reference sources. Absolute accuracy of the blackbody references are estimated to be about 0.5 K, resolution accuracy about 0.35 K and calibration accuracy about 0.8 K. Corrections for water vapor and carbon dioxide attenuation as functions of viewing angles were made using a model of Price (1982), which calculates the temperature correction for water vapor and carbon dioxide attenuation for different viewing angles given a temperature and moisture sounding. Since all the flight data discussed in this paper refer to the 1500 m altitude passes, the total water vapor correction was only a few degrees K. Overall, the accuracy of the radiometer including atmospheric correction is felt to be about 1.0–1.5 K. Pixel size for the 1500 m flights was approximately 4 m in diameter at nadir; no corrections for pixel size as a function of viewing angle were made.

NDVI

The NS001 Thematic Mapper simulator (TMS) was used to measure shortwave spectral radiances from the C-130. Although having a similar resolution to that of the TIMS and an across-track scanning pattern, the instantaneous field of view and surface co-location was slightly different from the TIMS radiometer owing to different scan angles and swath widths. NDVI measurements were made using the formula:

$$\mathrm{NDVI} = (R_4 - R_3)/(R_4 + R_3) \tag{3}$$

where R_3 is the radiance from Channel 3 (wavelength band 0.633–0.697 μm and R_4 is that for Channel 4 (wavelength 0.767–0.910 μm). No corrections were made for solar elevation and radiometer viewing angles. Viewing angles, however, were all less than 30°. According to Paltridge and Mitchell (1989),

corrections to a nadir NDVI for NOAA satellites are less than 10% for viewing angles less than 30°.

Soil moisture

Eight gypsum block locations were installed at each of the two PSU field sites, Lubbon and Castelnau. Average and standard deviations of volumetric soil water contents (θ_v) were determined for each site at approximately 5, 10, 20 and 40 cm depth. In general, the standard deviation of θ_v was about ± 0.04. Although this is not an insignificant variation, it is very similar to the mean standard deviation obtained by Bell et al. (1980) for that of natural soils.

ANALYSES

General approach

Fractional vegetation cover and LAI are determined by matching simulated radiometric surface temperatures, vegetation fraction and LAI with measured values of NDVI and radiometric surface temperatures. Asymptotic limits for sunlit leaves and sunlit bare soil are determined by inspection of the distribution of NDVI vs. radiometric surface temperature. Asymptotic leaf and soil temperatures are used to solve for, respectively, the root zone and soil surface water contents and fractional vegetation cover using the CM. Spurious effects of mutual leaf shading and small-scale variations in soil moisture are largely ignored, although they can be assessed qualitatively from inspection of image products. We make no distinction between different types of crops (corn, soybeans) in either the modeling or the interpretation of the images.

Method

The significance of NDVI

The NDVI constitutes a very useful tool in the study of vegetation cover. Normalization of the radiance differences between spectral intervals on either side of the near-infrared reflectance discontinuity tends to reduce effects of changing sun or viewing angle. Importantly, the NDVI is known to be correlated with the green leaf area, such as the one-sided LAI (Tucker, 1979; Holben et al., 1980; Curran, 1983; Asrar et al., 1984; Best and Harlan, 1985; Gallo et al., 1985; Sellers, 1985; Hansen and Soegaard, 1987; Peterson et al., 1987; Nemani and Running, 1989a). Tucker (1979) and later Best and Harlan (1985) show that the optimum sensitivity to biomass and LAI can be found in the ratio of near infrared (0.70–0.80 μm) to red (0.63–0.69 μm) radiances, bands which are similar to those referred to above. When these ratios

are compared with actual field measurements the error in LAI is typically about ± 1.0 for a given site.

NDVI increases almost linearly with increasing LAI and then enters an asymptotic regime in which NDVI increases very slowly with increasing LAI. Curran (1983) points out that the latter asymptotic region pertains to a surface almost completely covered by leaves. Although there is some variation, an upper asymptote of NDVI vs. vegetation density or LAI usually occurs near 0.5–0.8 for dense vegetation. This upper limit, however, is rather variable and depends on vegetation type, age, and leaf water content (Paltridge and Barber, 1988). For bare soil NDVI tends to vary between -0.1 and 0.2.

Curran also shows that the asymptotic region for LAI begins at values of 3–4 for short crops such as wheat, corn, sorghum and various grasses. Asymptotic regimes for LAI were found by Tucker (1979), Holben et al. (1980) for soybeans (above 2), Asrar et al. (1984) for wheat (above 2.5), Best and Harlan (1985) for oats (above 2), Gallo et al. (1985) for corn (above 3) and Sellers (1985) for various idealized canopies (above values from 1 to 3, depending on leaf angle). Nemani and Running (1989a) show that the change in LAI is nearly linear with NDVI until the former exceeds values of 3–4, above which NDVI rapidly approaches an asymptotic limit. In some conifers, however, the asymptotic region is at large values of LAI, such as in the study of Peterson et al. (1987), who found that the asymptotic domain was in excess of LAI = 6. Such large values of LAI are found on trees with large numbers of clumped needles.

Both Curran (1983) and Asrar et al. (1984) discuss contributions to the reflected radiance from leaves and from the underlying soil surface. They suggest that the asymptotic regime for LAI is one in which the reflectance from soil beneath the vegetation becomes very small. Alternatively stated, the asymptotic part of the LAI vs. NDVI curve occurs when the vegetation cover is close to 100%. Above an LAI of 3.0, little increase occurs in the fraction of bare soil visible to the radiometer. A modeling assumption used to obtain the vegetation fraction (f_v) is that solid vegetation cover ($f_v = 1.0$) begins at LAI = 3.0. LAI can increase above 3.0 but f_v remains at 1.0. Exact choice of the value of LAI for which $f_v = 1.0$ is not critical insofar as the sensitivity of the results is concerned. We found by trial and error that LAI = 3 for the threshold of solid vegetation yielded optimum agreement with HAPEX measurements. Another value might be more appropriate for other types of vegetation, such as trees.

The vertical variation of soil moisture at Lubbon

Figure 3 is a composite of measurements showing the vertical profile of soil water content for 16 June at Lubbon. Despite considerable scatter, it is clear that the deeper substrate (below about 10 cm) is relatively moist ($\theta_v = 0.2$), while the surface is very dry ($\theta_v = 0.02 - 0.06$). It should be noted that all of

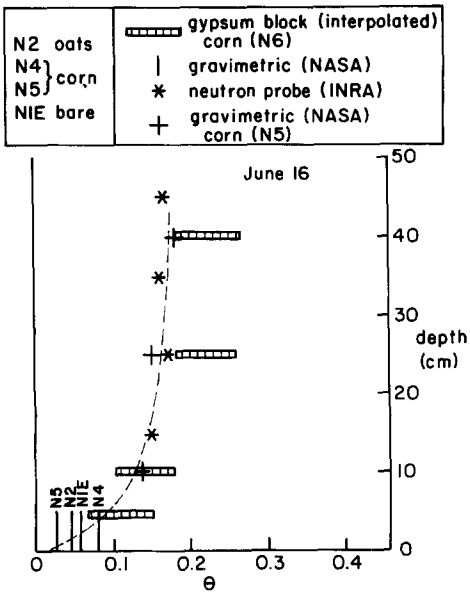

Fig. 3. Vertical profile of volumetric soil water content (θ_v) vs. depth in cm measured by different devices on 16 June 1986 at Lubbon.

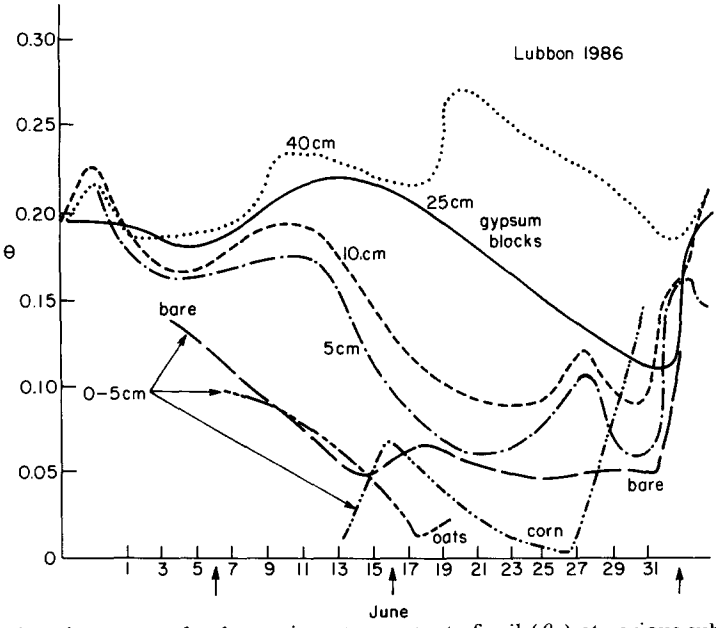

Fig. 4. Variations in measured volumetric water content of soil (θ_v) at various substrate levels during June 1986 at Lubbon. The 5, 10, 25 and 40 cm curves represent measurements made with gypsum blocks in the N6 corn field. The 0–5 cm curves are from gravimetric samples in the oat (N2), corn (N6) and bare (N1) fields at Lubbon.

the gravimetric measurements show a marked soil surface dryness after the early part of June until after 23 June (Fig. 4). By contrast, the deeper substrate remained fairly moist, but with some decrease in the 5 and 10 cm values of θ_v between 10 and 19 of June. Some irrigation was carried out on and after 23 June owing to lack of precipitation during the first three weeks of the month. Despite the irrigation and some minor rainfall episodes during the last few days of June, the large vertical soil water content gradient was present as late as 27 June. By early July, surface soil water contents had increased toward those at deeper levels.

Thermal imagery

Figure 5 is a thermal image made from digital scan data from the C-130 aircraft over the Lubbon region. Here, temperature is represented by a gray scale shading, dark representing cooler temperatures and light warmer temperatures. Field N6, consisting of corn about 0.8 m high with an LAI of 1.8, was the location of the Penn State measurement operation. The average temperature of this field was about 47°C. In contrast, Field N2 contained oats with a temperature of about 28°C, while Field N4 with newly planted corn and Field N1, which was bare, exhibit radiometric surface temperatures well in excess of 50°C. This image clearly shows the large differences in radiometric surface temperatures between the exposed sunlit bare soil areas and the

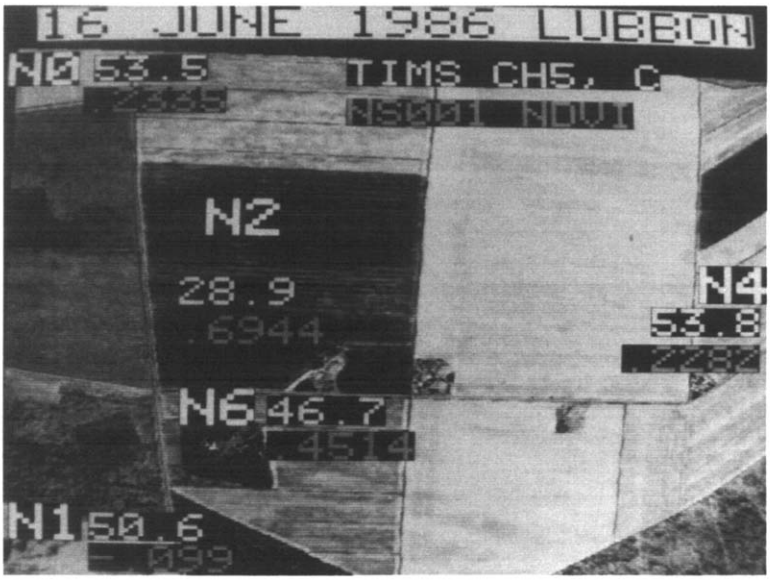

Fig. 5. TIMS thermal infrared image made from NASA C-130 flying at 1500 m on 16 June 1986 near Lubbon. Dark is cool and light is warm. Field numbers are indicated and field averages of temperature (°C) and NDVI are listed.

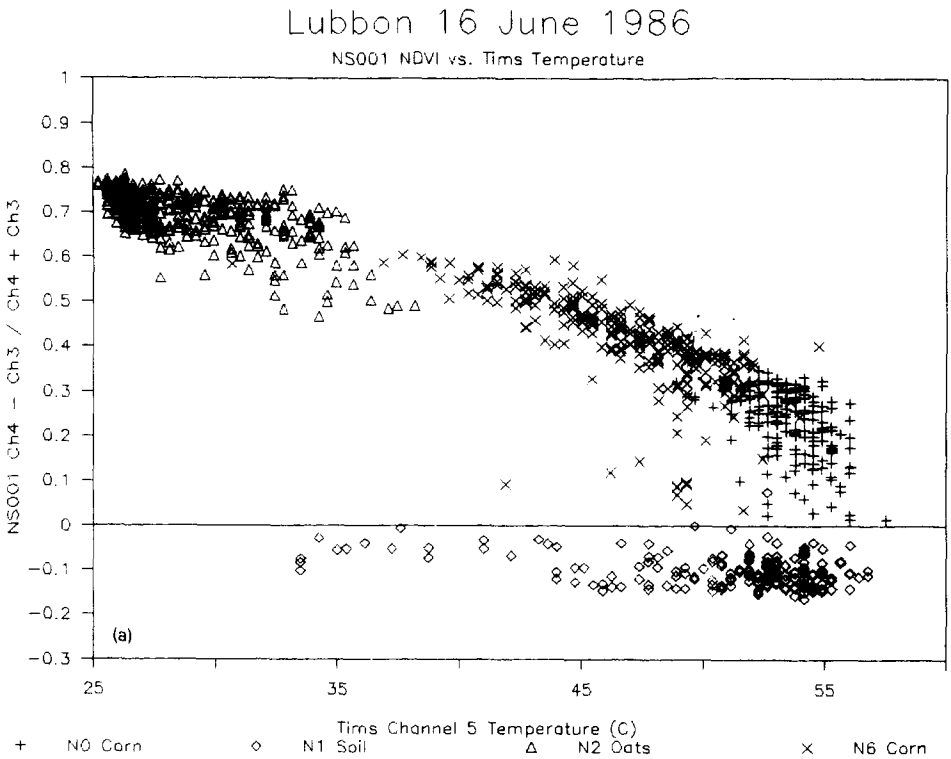
Lubbon 16 June 1986
NS001 NDVI vs. Tims Temperature
NS001 Ch4 - Ch3 / Ch4 + Ch3
(a)
Tims Channel 5 Temperature (C)
+ N0 Corn
◇ N1 Soil
△ N2 Oats
× N6 Corn

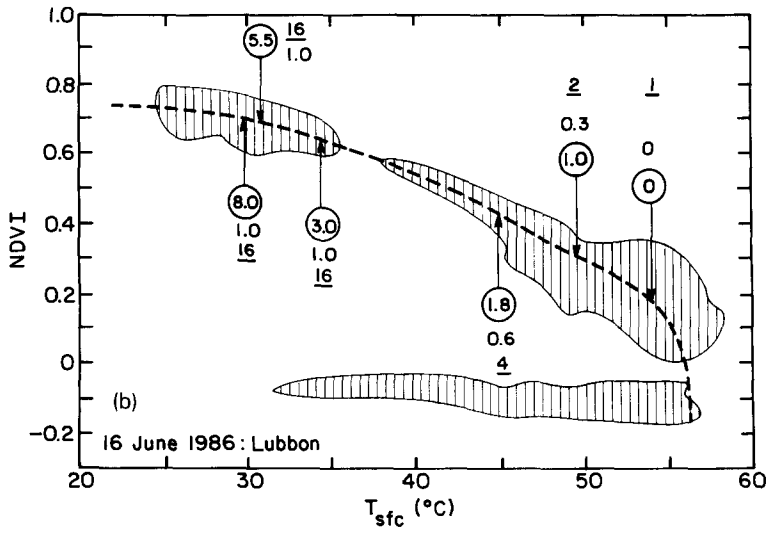
NDVI
(b)
16 June 1986 : Lubbon
T_{sfc} (°C)

vegetation, which is uniformly dark. It indirectly reflects the large vertical variation in soil dryness between the surface and substrate shown in Figs. 3–4.

Large temperature differences between vegetation and bare soil occurred on all 4 days in which temperature images were made. While less bare soil is visible on 27 June (figure not shown) than on 16 June (Fig. 5), the distribution of warm bare soil and cool vegetation temperatures are similar. By contrast, however, images for 6 June and 2 July (not shown) respectively exhibit small and large fractions of vegetation.

Combining NDVI and thermal measurements

Spatial variations in surface radiometric temperature, such as shown in Fig. 5, are related to variations in the vertical variation of soil water content modulated by fractional vegetation cover. The relationship between radiometric surface temperature and vegetation amount is illustrated in Figs. 6–9. Symbols plotted on the figures pertain to individual resampled pixels. The best example is that of 16 June, which is shown in Fig. 6. Data fall into two general clusters. One cluster contains positive values of NDVI in an envelope that slopes from the upper left-hand to lower right-hand sides of the NDVI/T_c distribution (Fig. 6a). The other cluster comprises points scattering horizontally and having negative values of NDVI. The sloping region extends from cool temperatures and high NDVI over the oat field (Field N2) to very high temperatures and low values of NDVI over newly planted corn fields (Field N0).

The figures exhibit a remarkable range of surface temperatures, with very warm values over bare or nearly bare soil. In the sloping distribution, pixels with high NDVI (in excess of 0.6) and low temperatures represent the asymptotic region in which the temperature approaches that for a sunlit leaf; (shaded leaves would be somewhat cooler but with approximately the same NDVI). At this end of the distribution, the upwelling long-wave radiation from the soil is almost totally attenuated. Large NDVI values for the oats probably correspond to an LAI well in excess of 3.0 and a vegetation fraction of 1.0. At the other end of the distribution, the very warm temperatures correspond to virtually bare soil with LAI almost equal to 0 and a zero vegetation fraction.

Fig. 6a. Distribution of NDVI vs. radiometric surface temperature (°C, corrected for atmospheric attenuation) for individual pixels over the scene in Fig. 5. The type of vegetation planted in each field is indicated by a symbol defined below the figure.

Fig. 6b. Same as Fig. 6a but in schematic form to show how the axis of variation (dashed line) was constructed from the data in Fig. 6a. Circled numbers are the values of LAI determined with the aid of the boundary layer model by matching observed and simulated temperatures given the surface and root-zone moisture contents. Decimal number represents the fractional vegetation cover, circled numbers the derived LAI, and the underlined number the value of surface roughness (cm) used in the model for that simulation.

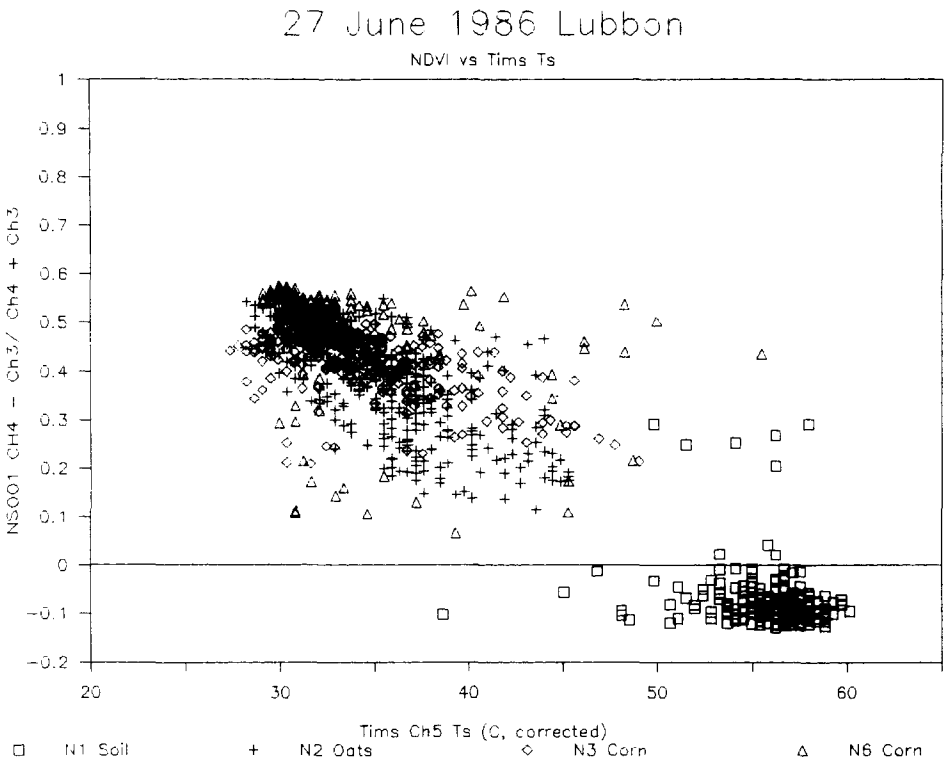

Fig. 7. Same as Fig. 6a but for 27 June.

Two other features in Figs. 6–9 are worth noting: one is a horizontal scatter of surface temperature, a cluster of pixels with a constant NDVI (e.g. the horizontal width of the envelope of data points in Fig. 6a). This cluster is probably associated with spatial variations in soil moisture and to variable effects of the canopy architecture, e.g. mutual shading of leaves. The second feature is the apparent decrease in the maximum NDVI with time between 6 June and 2 July. This trend may be due to changes in vegetation color with age.

Goward et al. (1985) and Nemani and Running (1989b) have proposed that NDVI/T_c diagrams can be used to infer vegetation amount or canopy resistance. The axis of the sloping distribution of points in Figs. 6–9 defines the variation of vegetation fraction with surface radiometric temperature. Providing that there is not a great deal of noise and the distribution of points exhibits a definable slope over a wide range of NDVI, one can define an "axis of variation" through the center of the sloping distribution of points, which, in this case, connects the mean values of T_c and NDVI for each field. This axis describes a spectrum of temperatures and NDVI values with visible bare soil fractions varying from almost zero to virtually 100% cover. For the sake

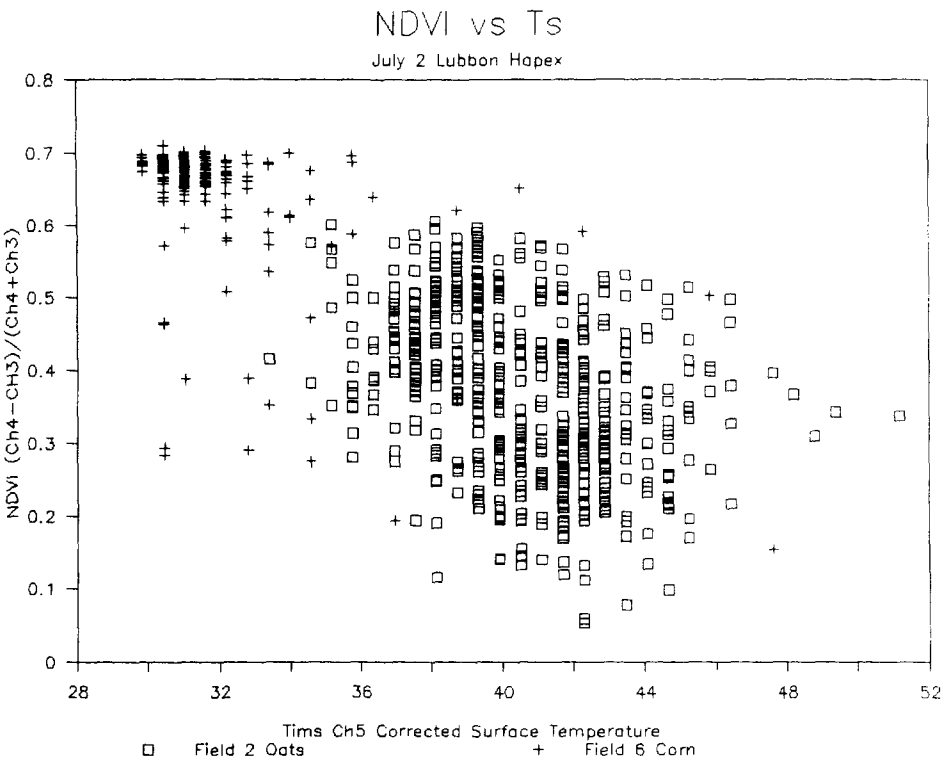

Fig. 8. Same as Fig. 6a but for 2 July.

of illustration, the axis of variation for Fig. 6a is shown by itself in Fig. 6b, but superimposed on a schematic background of pixel represented by hatching.

The NDVI/T_c distribution was less coherent on 27 June (Fig. 7) than on 16 June, although the variation in surface temperature was as large. A gap exists in the axis of variation at high surface temperatures and low values of NDVI owing to the relatively few bare soil patches between the plants. The separate cluster of bare soil temperatures, representing bare fields, is still present.

Field N6 was relatively cool and verdant on 2 July. Considerable scatter in the NDVI/T distribution (Fig. 8) may have been caused by the effects of irrigation, which was administered unevenly, and to ripening or senescence of the oats. Consequently, no axis of variation could be drawn with much confidence.

Most of the fields on 6 June were bare. The NDVI/T_c distribution (Fig. 9) for that date shows a horizontal variation of radiometric surface temperature along the zero NDVI axis, with one isolated cluster of pixels at NDVI = 0.6 and 10 °C. No axis of variation could be drawn with any confidence.

An oddity of Fig. 6 is the presence of a separate horizontally distributed

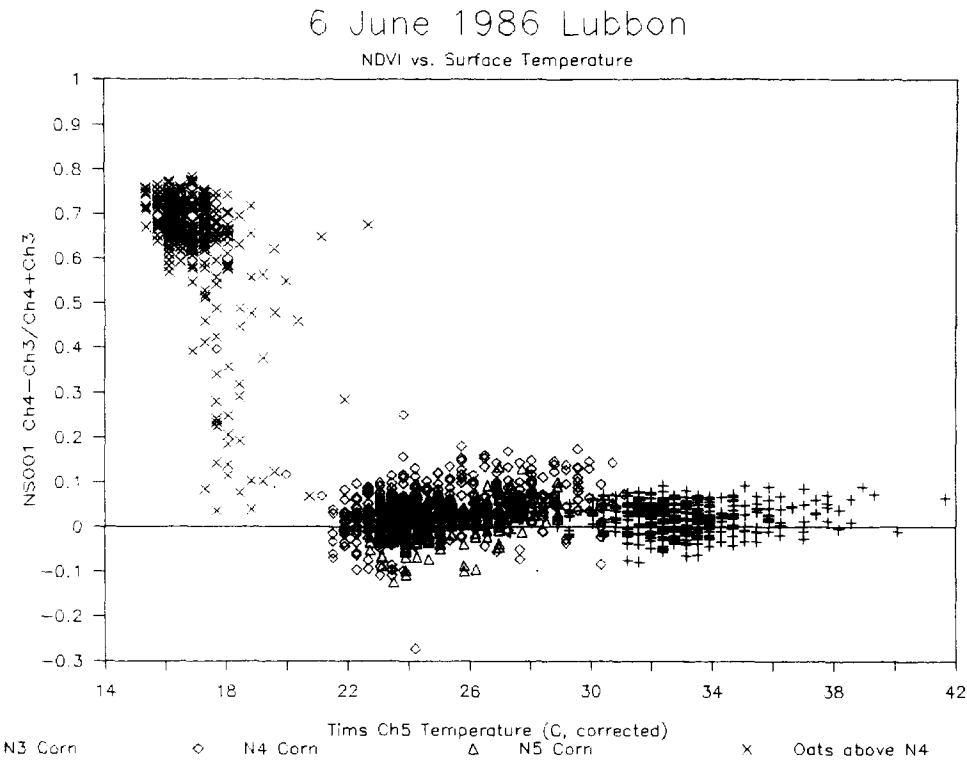

Fig. 9. Same as Fig. 6a but for 6 June.

cluster of pixels near or below the zero NDVI axis. This cluster represents pixels from unplanted or newly planted fields without vegetation, as distinct from bare soil patches between plants in fields that contain maturing vegetation. The reason for this difference is that freshly plowed bare fields would exhibit clods of relatively wetter earth interspersed with fragments of very dry surface soil, whereas bare soil between the plants would be dryer and littered with dead plant debris.

Interpretation of the imagery using a boundary layer model

Based on the assumptions described above, fractional vegetation as a function of NDVI or surface temperature was derived with the aid of the boundary layer model according to the following procedure.

First, asymptotic temperature extrema were determined for sunlit bare soil and sunlit leaf temperatures with the aid of the NDVI/T_c distribution (Figs. 6–9) and the "arch diagram". The arch diagram was originally developed by Coakley and Bretherton (1982) to analyze cloud cover in partially filled fields of view and later used by Albrecht et al. (1988) to separate sea surface temperatures from those at the top of marine stratus clouds. Figures 10–12 show

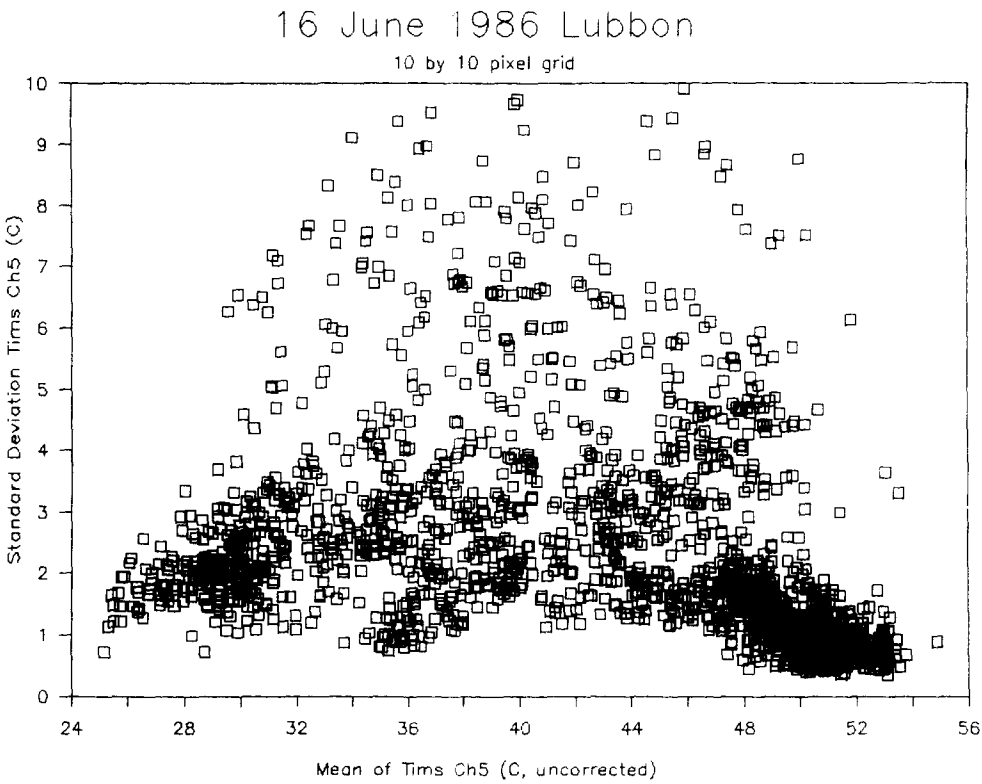

Fig. 10. The arch diagram: standard deviation of radiometric surface temperature vs. uncorrected radiometric surface temperature (°C) for 16 June at Lubbon (the image in Fig. 5). Each data point represents a sub-area consisting of about 10×10 original pixels.

the arch diagrams for 16 and 27 June and 2 July. The arch diagram consists of the standard deviation of temperature (in 10×10 pixel subsets) of the image vs. radiometric surface temperature averaged over that subset. No correction was made for viewing angle or for atmospheric attenuation. The two "feet" of the arch, characterized by dense clusters of relatively low standard deviations, suggest areas of uniform vegetation and bare soil temperatures, which correspond to the temperature extrema along the axis of variation in the NDVI/T_c distribution (e.g. Fig. 6b).

The second step was to use the boundary layer model to calculate substrate water content using the asymptotic temperatures. Thus the water contents (θ_{vo}; θ_v), pertain, respectively, to sunlit bare soil ($f_v=0$; LAI=0; $T_c=55\,°C$) and sunlit vegetation ($f_v=1.0$; $T_c=28\,°C$). Solutions are obtained by forcing agreement between simulated and measured surface temperatures at flight time (11:30 LST) (Table 1) for bare soil and solid vegetation.

The third step was to use these derived substrate water contents to calculate f_v as a function of surface radiometric temperature. In these simulations, LAI

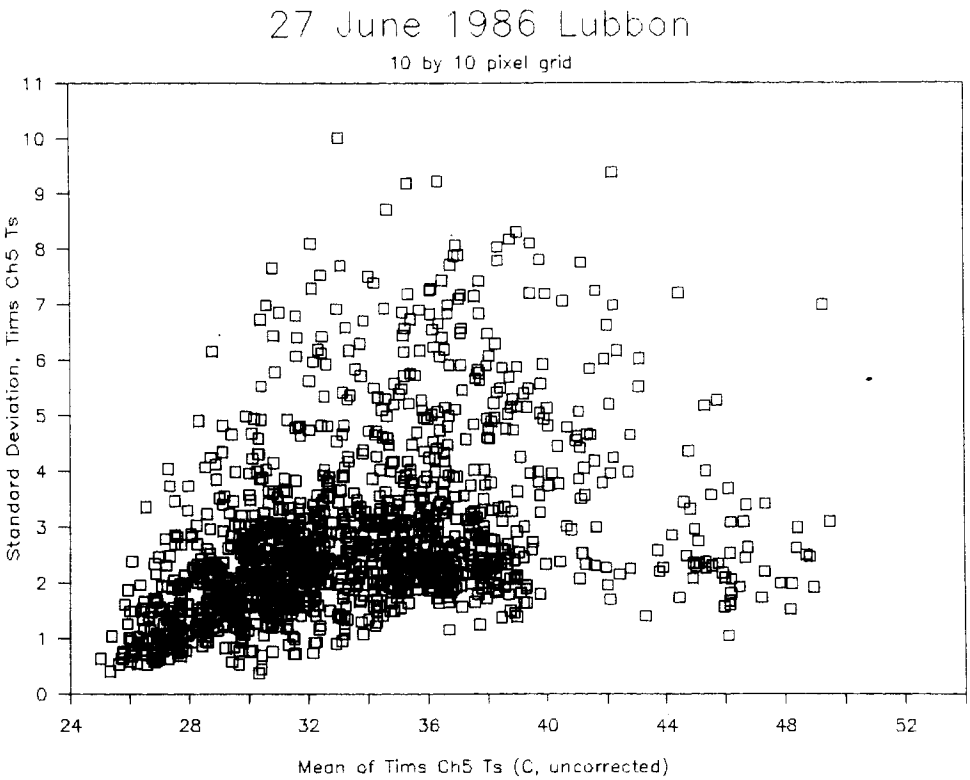

Fig. 11. Same as Fig. 10 but for 27 June.

is fixed at 3.0 for the vegetation fraction and 0 for the bare soil fraction (Fig. 1). We force the simulated and measured radiometric surface temperatures to agree along the axis of variation for different values of f_v in the model. Results are not sensitive to the choice of the solid vegetation value for LAI since the model is used only to convert a given temperature range to a fraction (f_v) between 0 and 1.0. Given f_v vs. T_c, one obtains the distribution of NDVI vs. f_v from the NDVI/T_c diagram. Figure 6b shows the values of LAI, f_v and surface roughness used to simulate temperatures along the axis of variation on 16 June. For example, given LAI = 1.8 (Field N6) the radiometric surface temperature is about 46 °C, the NDVI is about 0.4 and $f_v = 0.6$.

A final step was to perform a simulation to generate a range of surface radiometric temperatures as LAI varies above 3.0 with $f_v = 1.0$. This operation simply allows us to determine LAI as a function of radiometric temperature for the solid cover, but has no bearing in determining f_v. Similar calculations were made for 27 June.

At this point, it is possible to specify vegetation fraction (f_v between 0 and 1.0) and the average value of LAI for each resampled pixel, given its measured values of radiometric surface temperature and NDVI. From this information one calculates the fluxes of sensible and latent heat for each pixel.

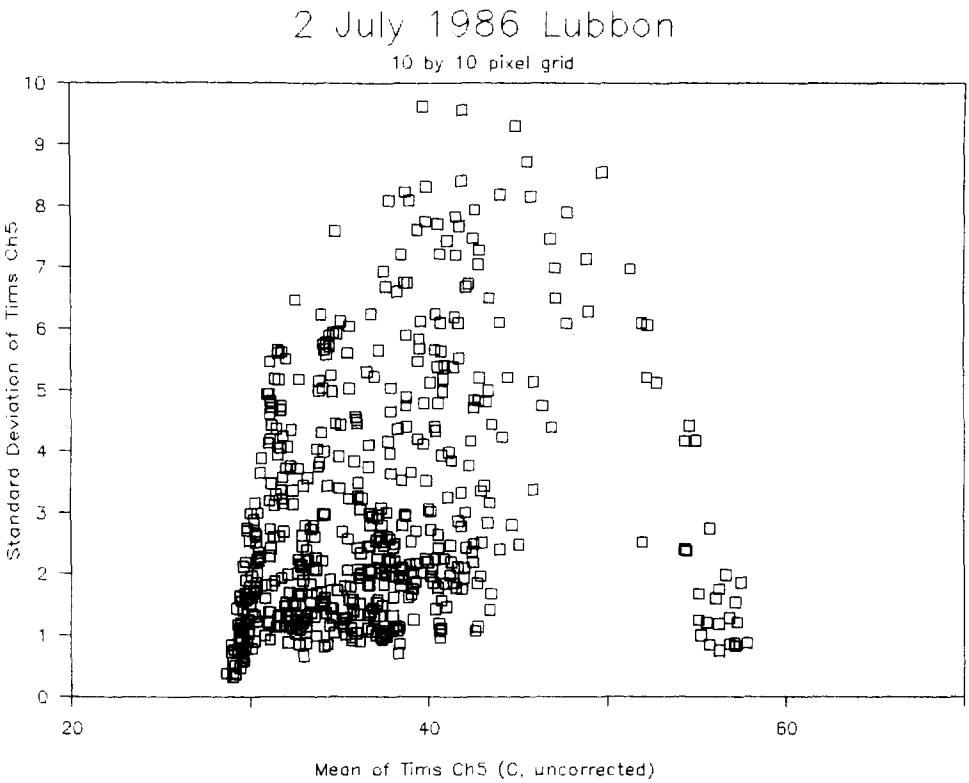

Fig. 12. Same as Fig. 10 but for 2 July.

TABLE 1

Average values of measured and derived quantities for Field N HAPEX (Lubbon), 1986

	LAI(m)[a]	LAI	f_v	T_c(m) (°C)	T_{bare} (°C)	T_{veg} (°C)	NDVI(m)	θ_{vo}	θ_v
6 June[b]	0.6	–	–	–	–	–	–	–	–
16 June	1.8	1.8	0.6	46	55	30	0.45	0.01	0.22
27 June	3.2	3	1.0	33	(48)[c]	33	0.48	0.01	0.22
2 July	3.7	5	1.0	32	(58)	32	0.64	0.01	0.17

[a]m = measured; [b]No aircraft measurements made over Field N6; [c]Values in parentheses are uncertain.

DISCUSSION

Results of simulations

Not surprisingly, the high temperature asymptote corresponds to a low soil

surface water content ($M_o = 0.02$; $\theta_v = 0.006$). We were unable to simulate the highest temperatures without specifying a very low thermal inertia, appropriate to the sandy soil of Lubbon. Simulations for wet soil show little variation in temperature as a function of M between $M = 0.6$ and $M = 1.0$ (θ_v between 0.21 and 0.34). Thus, it was more difficult to simulate precisely the root zone water content at the cool end of the axis of variation, since surface temperature is insensitive to substrate water content in wet conditions. Accordingly, we chose to let $M = 0.65$ and $\theta_v = 0.22$ for both 16 and 27 June, values corresponding to those measured in the root zone (Figs. 3–4).

Simulations were made for the bare soil cluster (NDVI less than zero). These showed that the surface moisture availability (M_o) varied from about 0 to 0.6 between the warm and cool temperatures.

Asymptotic temperatures on 27 June were approximately the same as on 16 June, although it was more difficult to derive a bare soil asymptote on 27 June because of greater scatter and a gap in the measured NDVI/T_c distribution. The arch diagram (Fig. 11) for 27 June suggests a small amount of dry, bare soil with temperatures approaching 60°C, but the NDVI/T_c distribution does not lend confidence in determining the warm end of the axis of variation. (Recent evidence published by the French indicates that the measured temperatures from TIMS are too warm, perhaps by as much as several °C for the high temperatures. This error is due to deterioration in the block body target in the radiometer. See: M. Stoll, Temperature de Surface restituee a partir du radiometre aeroporte T.I.M.S. Rapport de stage effective au CNRM, Toulouse, 29 June 1989 promotion I.M. 87/89, 56 pp.) Simulations for 27 June yield similar results to those of 16 June, which is not surprising in view of the fact that the NDVI/T_c distributions appear to be similar. However, we cannot explain why the axis of variation was at lower values of NDVI on 27 than on 16 June (Fig. 7).

Simulations for 6 June show that the surface moisture availability (M_o) varied from about 1.0 on the cool side to about 0.1 ($\theta_v = 0.03$) on the warm side of this cluster of bare soil temperatures. Surface temperatures were not as warm as during late June, although a few pixels were extremely hot. The isolated cluster of cool pixels in Fig. 9, which represent the oats canopy, could not be simulated without reducing the solar flux intensity below that for clear skies. This suggests that these pixels may have been partly shaded by leaves or by cloud.

Although no axis of variation was obtainable for 2 July because of the enormous amount of scatter, the NDVI/T_c distribution does suggest that the warmest soil temperatures were about 45°C, the equivalent in the model of a surface moisture availability (M_o) of about 0.1. These values reflect the somewhat higher surface soil moisture contents found on this day (as compared with 16 June); the arch diagram indicates that there were still some very high surface temperatures corresponding to almost zero surface moisture availability in some bare patches.

Table 1 summarizes some results for Field N6. Presented are values of LAI (measured), LAI (derived), f_v (derived), NDVI (measured) and the pure sunlit leaf and sunlit bare soil temperatures (LAI = 3.0 and 0) and for the appropriate field average of LAI which allows measured and simulated surface temperature to agree. Also shown are simulated root zone water contents. The last two days constitute 100% canopy cover for Field N6 (LAI exceeding 3.0), whereas 16 June is an example of partial vegetation cover in a single field.

Comparison with measurements

Some independent confirmation of the results can be made by comparing the measured values of LAI and NDVI with the simulated values of NDVI and LAI as a function of simulated vegetation fraction (f_v). LAI was measured at the PSU site in Field N6 on four occasions during the same period. Figure 13 shows the distribution of measured NDVI vs. measured LAI and the derived NDVI (from the axes of variation) as simulated by the model. The comparison is obviously very good for 16 June but agreement with measurements is not as close for 27 June because of greater scatter in the data (Fig. 7). Had we chosen a somewhat smaller LAI threshold for solid vegetation than 3.0, agreement between measured and modelled LAI would have been closer to the measured LAI on 27 June.

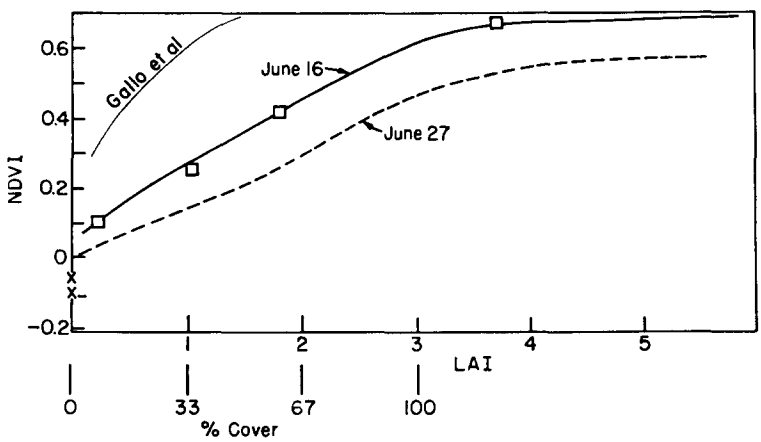

Fig. 13. NDVI vs. percent cover and LAI for model simulations for 16 June and 27 June at Lubbon. Squares represent simultaneous aircraft measurements of NDVI and ground measurements of NDVI made on 4 days over the Lubbon field (N6) during June; crosses represent measured NDVI and LAI for almost bare soil. Heavy solid line represents simulated LAI and fraction vegetation cover vs. NDVI, consistent with axis of variation for measurements. The thin solid line obeys a formula proposed by Gallo et al. (1985) for NDVI vs. LAI over corn.

Problems in applying the method

The difficulty in determining the axis of variation, especially on 6 June and 2 July underscores the central problem in this method. To some extent, poorer agreement with measurements on 27 June, as compared with 16 June, is due to the wide horizontal scatter of points and the lack of values on the warm side of the axis of variation. Clearly, the distribution of points on 16 June is ideal, because the variance of temperature at constant NDVI is quite small.

The derived fractional vegetation cover depends on the architecture of vegetation, the geometry of bare soil distribution, the type of soil and vegetation and the solar and radiometer viewing angles; f_v will tend to increase with increasing solar or viewing angles. The present results, however, suggest that various crops can be combined to produce a meaningful axis of variation. However, extending the method to a mixture of trees and crops may prove untenable.

A difficulty in applying the method would be encountered with regard to satellite measurements because of their relatively low resolution. Instruments such as the AVHRR (1 km resolution) may be incapable of producing a wide range of NDVI and surface temperature over a target area. Thus, it may be necessary to extrapolate the axis of variation and to composite satellite measurements over successive images. Nemani and Running (1989b) have recently presented some encouraging results showing that the AVHRR is capable of determining an axis of variation over forests. Their figures show that the slope of the axis of variation varies according to the amount of surface moisture.

SUMMARY

This study suggests a method to derive a spatial distribution of fractional vegetation cover and soil moisture in the surface and root zone over patchy or sparse vegetation. The method makes use of two types of image products: the distribution of NDVI vs. radiometric surface temperature (the NDVI/T_c) and the "arch" diagram, which shows the distribution of radiometric surface temperature in subgroups of pixels vs. the standard deviation of the radiometric surface temperature in those subgroups. These two diagrams aid in identifying asymptotic limits of the sunlit leaf and the sunlit bare soil temperature. It also allows one qualitatively to assess the degree of noise produced by small-scale variations in soil moisture and leaf shading.

The boundary layer model is used to estimate soil surface and root zone water contents, given the asymptotic vegetation and bare soil temperatures. A crucial aspect of the method is to define the relationship between NDVI and surface radiometric temperature, which we call axis of variation. From this, we obtain average soil moisture values for surface and root zone, and a

vegetation fraction, surface turbulent heat fluxes and LAI as functions of NDVI for each pixel.

Some subjectivity is inherent in the method. An axis of variation may not always be easy to define, for example when small-scale variations in soil moisture are large (perhaps owing to irrigation), where the amount of bare soil is negligible or where the soil surface temperature and leaf temperatures are similar, as in the case of wet soil. Large horizontal variations in soil moisture increase the scatter. Nevertheless, even when the axis of distribution is obscured because of noise, the NDVI/T_c and arch diagrams yield useful qualitative information on the distribution of vegetation cover, small-scale variations in soil moisture and vertical gradient of soil water content. A reliable axis of variation could be determined by compositing measurements obtained from a sequence of images.

The method needs to be tested on many types of soils and vegetation. Application to analysis of AVHRR satellite data may prove useful over different types and mixes of vegetation, although it is still too early to determine if lower-resolution satellite radiometers can define a usable axis of variation.

ACKNOWLEDGEMENTS

The authors would like to thank the sponsors of this research, the National Aeronautics and Space Administration under grant NAG 5-919, the United States Geological Survey under grant no. 14-08-0001-G1490, and the United States Department of Agriculture/Agriculture Research Service under grant no. 58-32U4-8-27.

REFERENCES

Andre', J.C., et al., 1988. Evaporation over land surfaces: First results from HAPEX-MOBILHY special observing period. Ann. Geophys., 6: 477–492.

Asrar, G., Fuchs, M., Kanemasu, E.T. and Hatfield, J.L., 1984. Estimating absorbed photosynthetic radiation and leaf area index from spectral reflectance in wheat. Agron. J., 76: 300–306.

Albrecht, B.A., Randall, D.A. and Nicholls, S., 1988. Observations of marine stratocumulus clouds during FIRE. Bull. Am. Meteorol. Soc., 69: 618–626.

Bell, K.R., Blanchard, B.J., Schmugge, T.J. and Witzak, M.W., 1980. Analysis of surface moisture variations within large field sites. Water Resour. Bull., 16: 796–810.

Best, E.G. and Harlan, J.C., 1985. Spectral estimation of green leaf area index of oats. Remote Sensing Environ., 17: 27–36.

Carlson, T.N. and Boland, F.E., 1978. Analysis of urban–rural canopy using a surface heat flux/temperature model. J. Appl. Meteorol., 17: 998–1013.

Carlson, T.N., Dodd, J.K., Benjamin, S.G. and Cooper, J.N., 1981. Remote estimation of surface energy balance, moisture availability and thermal inertia. J. Appl. Meteorol., 20: 67–87.

Coakley, J.A. and Bretherton, F.P., 1982. Cloud cover from high resolution scanner data: Detecting and allowing for partially filled fields of view. J. Geophys. Res., 87: 4917–4932.

Curran, P.J., 1983. Multispectral remote sensing for the estimation of green leaf area index. Philos. Trans. R. Soc. London, Ser. A., 309: 257–270.

Gallo, T.F., Daughtry, C.S.T. and Bauer, M.E., 1985. Spectral estimation of absorbed photosynthetically active radiation in corn canopies. Remote Sensing Environ., 17: 221–232.

Goward, S.N., Cruickshanks, G.D. and Hope, A.S., 1985. Observed relation between thermal emission and reflected radiance of a complex vegetated landscape. Remote Sensing Environ., 18: 137–146.

Hansen, B. and Soegaard, H., 1987. Monitoring vegetation index and biomass production in southern Greenland based on NOAA-AVHRR data. 21st International Symposium on Remote Sensing of Environment, Ann Arbor, MI, 26–30 October 1987. 10 pp.

Hatfield, J.L., Reginato, R.J. and Idso, S.B., 1984. Evaluation of canopy temperature-evapotranspiration models over various crops. Agric. For. Meteorol., 32: 41–53.

Holben, B.N., Tucker, C.J. and Fan, C-J., 1980. Spectral assessment of soybean leaf area and leaf biomass. Photogramm. Eng., 46: 651–656.

Idso, S.B., Schmugge, T.J., Jackson, R.D. and Reginato, R.J., 1975. The utility of surface temperature measurements for remote sensing of soil water studies. J. Geophys. Res., 80: 3044–3049.

Jackson, R.D., 1982. Canopy temperature and crop water stress. In: D. Hillel (Editor), Advances in Irrigation. Academic Press, Vol. 1, pp. 43–85.

Jackson, R.D., Reginato, R.J. and Idso, S.B., 1977. Wheat canopy temperature: A practical tool for evaluating water requirements. Water Res. Manage., 13: 651–656.

Lagouarde, J.P. and Choisnel, E., 1990. A new agrometeorological model for evaporation and surface temperature. Agric. For. Meteorol, submitted.

Monteith, J.L., 1975. Vegetation and the Atmosphere, Vol. I, Academic Press, New York, NY, 278 pp.

Nemani, R.R. and Running, S.W., 1989a. Testing a theoretical climate–soil–leaf area hydrological equilibrium of forests using satellite data and ecosystem simulation. Agric. For. Meteorol., 44: 245–260.

Nemani, R.R. and Running, S.W., 1989b. Estimation of regional surface resistance to evapotranspiration from NDVI and Thermal-IR AVHRR data. J. Appl. Meteorol., 28: 276–284.

Paltridge, G. and Barber, J., 1988. Monitoring grassland dryness and fire potential in Australia with NOAA/AVHRR data. Remote Sensing Environ., 28: 384–393.

Paltridge, G. and Mitchell, R.M., 1989. Atmospheric and viewing angle correction of vegetation indices and grassland soil moisture content derived from NOAA/AVHRR data. Remote Sensing Environ., in press.

Peterson, D.L., Spanner, M.A., Running, S.W. and Teuber, K.B., 1987. Relationship of thematic mapper simulator data to leaf area index of temperate coniferous forests. Remote Sensing Environ., 22: 323–341.

Price, J.C., 1982. On the use of satellite data to infer surface fluxes at meteorological scales. J. Appl. Meteorol., 21: 1111–1122.

Raffy, M. and Becker, F., 1985. An inverse problem for remote sensing in the thermal infrared bands and its solution. J. Geophys. Res., D3(90): 5809–5819.

Schmugge, T., 1978. Remote sensing of surface soil moisture. J. Appl. Meteorol., 17: 1549–1557.

Schmugge, T.J. and Janssen, L., 1988. Aircraft remote sensing in HAPEX. Procedures of the 4th International Colloqium on Spectral Signatures in Objects of Remote Sensing. Aussois, France, 18–22 June 1988, (ESA SP-287), pp. 463–467.

Sellers, P.J., 1985. Canopy reflectance, photosynthesis and transpiration. Int. J. Remote Sensing, 6: 1335–1372.

Shuttleworth, W.J. and Wallace, J.S., 1985. Evaporation from sparse crops – an energy combination theory. Q. J. R. Meteorol. Soc., 111: 839–855.

Taconet, O., Carlson, T.N., Bervard, R. and Vidal-Madjar, D., 1986. Evaluation of a surface/vegetation parameterization using satellite measurements of surface temperature. J. Climate Appl. Meteorol., 25: 1752–1767.

Tucker, C.J., 1979. Red and photographic infrared linear combinations for monitoring vegetation. Remote Sensing Environ., 8: 127–150.

Wetzel, P.J. and Woodward, R.H., 1987. Soil moisture estimation using GOES-VISSR infrared data: A case study with a simple statistical method. J. Climate Appl. Meteorol., 26: 107–117.